

1 **Vertical changes in volatile organic compounds (VOCs) and**
2 **impacts on photochemical ozone formation**

3 Xiao-Bing Li¹, Bin Yuan^{1,*}, Yibo Huangfu¹, Suxia Yang², Xin Song¹, Jipeng Qi¹,
4 Xianjun He¹, Sihang Wang¹, Yubin Chen¹, Qing Yang¹, Yongxin Song¹, Yuwen Peng¹,
5 Guiqian Tang^{3,4}, Jian Gao⁵, Dasa Gu⁶, Min Shao¹

6 ¹ College of Environment and Climate, Institute for Environmental and Climate
7 Research, Guangdong-Hongkong-Macau Joint Laboratory of Collaborative Innovation
8 for Environmental Quality, Jinan University, Guangzhou 511443, China

9 ² Guangzhou Research Institute of Environment Protection Co., Ltd., Guangzhou
10 510620, China

11 ³ State Key Laboratory of Atmospheric Environment and Extreme Meteorology,
12 Institute of Atmospheric Physics, Chinese Academy of Sciences, Beijing 100029, China

13 ⁴ University of Chinese Academy of Sciences, Beijing, 100049, China

14 ⁵ State Key Laboratory of Environmental Criteria and Risk Assessment, Chinese
15 Research Academy of Environmental Sciences, Beijing 100012, China

16 ⁶ Guangdong–Hongkong–Macau Joint Laboratory of Collaborative Innovation for
17 Environmental Quality and Division of Environment and Sustainability, The Hong
18 Kong University of Science and Technology, Hong Kong 999077, China

19 * Corresponding author: Bin Yuan (byuan@jnu.edu.cn)

20 Abstract

21 Volatile organic compounds (VOCs) play crucial roles in regulating the formation
22 of tropospheric ozone. However, limited knowledge on the interactions between
23 vertical VOC variations and photochemical ozone formation in the planetary boundary
24 layer (PBL) has hindered effective ozone control strategies, especially in large cities.
25 In this study, we investigated the vertical changes in concentrations, compositions, and
26 key driving factors of a large suite of VOCs using online gradient measurements taken
27 from a 325 m tall tower in urban Beijing. ~~We also analyzed t~~The impact of these vertical
28 VOC variations on photochemical ozone formation were also analyzed using box
29 model simulations. Our results indicate that VOCs exhibited distinct vertical variation
30 patterns due to their differences in sources and chemical reactivities, ~~the vertical~~
31 ~~variations of various VOC species are strictly regulated by~~along with the diurnal
32 evolution of the ~~planetary boundary layer~~PBL. During daytime, reactive VOCs (e.g.,
33 hydrocarbons) are rapidly oxidized as they mix upwards, ~~leading accompanied by~~to the
34 formation and accumulation of oxygenated VOCs (OVOCs) in the middle and upper
35 layers. ~~— In addition~~~~This process plays a more significant role in regulating~~
36 ~~photochemical ozone formation with increasing height. In the lower layer,~~ the
37 photochemical formation of ozone responds positively to changes in both NO_x and
38 VOCs. As a result, the production rate of ozone ~~decreases~~declines with height due to
39 the simultaneous decreases in concentrations of reactive VOCs and NO_x ~~due to~~
40 ~~significant reductions in the concentrations of both NO_x and VOCs,~~ but remains high
41 in the middle and upper layers. The strong production of ozone aloft is primarily driven
42 by the presence of high OVOCs concentrations ~~of OVOCs and hydroxyl radicals, which~~
43 ~~can act as an important source of ozone at ground level.~~ Therefore, careful consideration
44 should be given to the vertical variations in both photochemical ozone production rates
45 and formation regimes in the whole PBL ~~boundary layer~~ when developing regional
46 ozone control strategies.

47 **1 Introduction**

48 Volatile organic compounds (VOCs) are crucial constituents of atmospheric
49 chemicals (*Li et al., 2022c*) and play important roles in regulating the atmospheric
50 oxidation capacity and contributing to the photochemical formation of tropospheric
51 ozone (*Zhao et al., 2022; Yang et al., 2024b*). Ozone is a major air pollutant in urban
52 environments, with increasing trends reported globally over recent decades (*Fleming et*
53 *al., 2018; Cooper et al., 2020*), despite stringent measures to control its precursor
54 emissions (*Wang et al., 2020b; Yeo and Kim, 2021; Li et al., 2022b; Perdignes et al.,*
55 *2022*). As highlighted in previous studies, reducing emissions of reactive VOCs is key
56 to controlling ozone pollution at present and in the foreseeable future (*Zhao et al., 2022;*
57 *Wang et al., 2024*).

58 The primary prerequisite for effective regional ozone pollution control is the
59 determination of the photochemical ozone formation regime (*Souri et al., 2020; Zhao*
60 *et al., 2022*), which facilitates the development of reduction schemes for key precursor
61 emissions (*Ou et al., 2016; Wang et al., 2019*). The main challenges in controlling
62 ozone pollution stem from the complex compositions of its precursors (e.g., VOCs and
63 NO_x) in ambient air (*Guo et al., 2017; Wu et al., 2020; Li et al., 2022c*), as well as the
64 complicated responses of photochemical ozone formation to changes in these
65 precursors (*Shao et al., 2021; Perdignes et al., 2022*). Furthermore, the interactions
66 between vertical variations of ozone precursors and ozone formation remain unclear
67 (*Tang et al., 2017; Sun et al., 2018; Li et al., 2024*), adding to the complexity of ozone
68 pollution control.

69 In most cases, the identification of key ozone precursors has been conducted using
70 ground-level observations (*Qi et al., 2021; Lu et al., 2022*) or compiled source emission
71 inventories (*Ou et al., 2015; An et al., 2021; Wang et al., 2022b*). While these methods
72 are undoubtedly helpful in determining key ozone precursors and corresponding
73 reduction strategies, they often encounter unexpected uncertainties in urban regions.
74 (*Mo et al., 2018; Mo et al., 2020*). Consequently, ground-level measurements of ozone

75 precursors have been favored to constrain model calculations (*Lu et al., 2012; Wang et*
76 *al., 2022a; Yang et al., 2022*) or provide empirical evidence for hypothesized theories
77 (*Hofzumahaus et al., 2009; Wang et al., 2022c*). However, these ground-level
78 measurements cannot fully characterize atmospheric chemical processes in the entire
79 planetary boundary layer (PBL) due to strong vertical variations in precursor
80 concentrations (*Velasco et al., 2008; Li et al., 2018; Sun et al., 2018*).

81 Ambient VOCs, as crucial ozone precursors, are composed of myriad species (*Wu*
82 *et al., 2020; Gkatzelis et al., 2021; Ye et al., 2021; He et al., 2022*) and serve diverse
83 functions in photochemical ozone formation (*Vo et al., 2018; Li et al., 2022a; Zhang et*
84 *al., 2022*). Owing to the impact of variations in emission sources, chemical removal,
85 advection and convection transport, and secondary formation, the concentration and
86 composition of VOCs typically display notable vertical variability within the PBL,
87 especially in urban areas (*Li et al., 2022c*). The ozone formation regime likely
88 undergoes significant transitions from the ground to the upper boundary layer (*Li et al.,*
89 *2024; Liu et al., 2024a*). Ozone generated throughout the PBL can influence surface
90 ozone levels due to enhanced atmospheric vertical mixing during the day. Consequently,
91 it is imperative to comprehend the vertical variations and principal determinants of
92 VOCs, as well as their effects on photochemical ozone formation within the PBL.

93 With the rapid development of cities in the recent two decades in China, a large
94 number of pollution-emitting industries and factories have been relocated from city
95 centers to alleviate air pollution. Concurrently, there's been a swift increase in the
96 ownership of electric vehicles (*Guo et al., 2021*). These shifts in energy consumption
97 have driven the change in concentrations and compositions of VOCs in major cities like
98 Beijing (*Liu et al., 2024b*), subsequently affecting photochemical ozone formation
99 (*Wang et al., 2024*). However, the vertical variations and key drivers of VOCs and their
100 impacts on photochemical ozone formation in the urban PBL remain elusive. A primary
101 hurdle in studying these vertical changes in photochemical ozone formation is the
102 scarcity of reliable vertical VOC data (*Dieu Hien et al., 2019; Li et al., 2022c*).
103 Engaging in vertical profiling of VOCs, ensuring all necessary species represented and

104 obtaining sufficient sample size, is especially challenging in the lower PBL where
105 atmospheric chemical reactions are most intense (*Benish et al., 2020; Kim et al., 2021*).

106 Previous studies on vertical distributions of photochemical ozone formation in the
107 PBL have been conducted using measurements of a limited number of VOC species
108 and samples (*Zhang et al., 2018; Benish et al., 2020; Geng et al., 2020*). In this study,
109 online gradient measurements of ozone, NO_x, and a large suit of VOCs were made on
110 a 325 m tall tower in urban Beijing during the summer of 2021. Additionally, box model
111 simulations constrained by the gradient measurements were performed to analyze the
112 vertical variations and key drivers of VOCs as well as their impacts on photochemical
113 ozone formation.

114 **2 Methods and materials**

115 **2.1 Description of the site, instrument, and field campaign**

116 The data utilized in this study was derived from an intensive field campaign
117 conducted at the Beijing Meteorological Tower (BMT: 39°58' N, 116°23' E) between
118 July 6 and August 4, 2021. The BMT has a height of 325 m and is located in the northern
119 part of downtown Beijing, positioned between the third and fourth ring roads (Fig. S1).
120 A vertical observation system, established using long perfluoroalkoxy alkane (PFA)
121 Teflon tubes (OD: 1/2 in.), was used to make online gradient measurements of ozone,
122 NO_x, and a set of VOCs on the BMT. Five specific heights, namely 15, 47, 102, 200,
123 and 320 m above ground level, were selected to mount the tube inlets, as depicted in
124 Fig. S2S3. An additional inlet, situated approximately 5 m above ground level, was
125 mounted on the rooftop of the observation room that was adjacent to the tower.
126 Consequently, the vertical observation system totally included a total of six sampling
127 inlets. The sampling inlet at the 15 m height was not utilized during this field campaign.

128 Filters were installed downstream of the tubing inlets on the tower to remove fine
129 particles. A rotary vane vacuum pump was used to simultaneously and continuously
130 draw sample air from the five tubes, ensuring that all tubes were flushed by ambient air

131 to reduce tubing delays of sticky organic compounds (*Pagonis et al., 2017; Liu et al.,*
132 *2019*). Five critical orifices were employed to control the flow rate of the air stream in
133 each tubing, resulting in flow rates ranging between 15 and 20 standard liter per minute
134 (SLPM). Instruments drew sample air from the five tubes sequentially through a Teflon
135 solenoid valve group at designated time intervals. The switching time intervals of the
136 Teflon solenoid valve group were set as 4 minutes during this field campaign. The
137 measurements of trace gases in the first and last 1 minute of a four-minute period were
138 discarded to eliminate cross interferences between different inlet heights. Detailed
139 information on the vertical observation system and the assessment of trace gas
140 measurements through hundreds of meters long PFA tubes has been provided in our
141 previous works (*Li et al., 2023; Song et al., 2024; Yang et al., 2024a*).

142 Ozone was measured using the ultraviolet photometry method (49i, Thermo Fisher
143 Scientific Inc., USA). NO, NO₂, and NO_x were measured using the chemiluminescence
144 method (42i, Thermo Fisher Scientific Inc., USA). Gradient measurements of ozone
145 and NO_x were conducted at a time resolution of 10 seconds. The photolysis frequencies
146 of NO₂, represented by $j(\text{NO}_2)$, were measured by a spectrometer (PFS-100, Focused
147 Photonics Inc., China) situated on the rooftop of the observation room and have a time
148 resolution of 8 seconds. In situ measurements of meteorological parameters including
149 wind speed, air temperature, and relative humidity were made at 15 heights between 8
150 m and 320 m on the BMT with a time resolution of 20 seconds. Planetary boundary
151 layer height (PBLH) was obtained from the Air Resources Laboratory
152 (<https://ready.arl.noaa.gov/READYamet.php>, last access: 10 June 2024) and was
153 linearly interpolated to hourly values based on the initial time resolutions of three hours
154 (*Li and Fan, 2022*).

155 A high-resolution proton-transfer-reaction quadrupole interface time-of-flight
156 mass spectrometer (PTR-ToF-MS, Ionicon Analytik, Austria) was employed to measure
157 VOCs at a time resolution of 10 seconds. The PTR-ToF-MS used both hydronium ion
158 (H₃O⁺) (*Yuan et al., 2017; Wu et al., 2020; Li et al., 2022c*) and nitric oxide ion (NO⁺)
159 (*Wang et al., 2020a*) as reagent ions. These two reagent ions were automatically

160 switched every 60 min for H_3O^+ and every 22 min for NO^+ throughout the campaign.
161 The PTR-ToF-MS operated at an E/N value of approximately 120 Td in H_3O^+ mode
162 and an E/N value of around 60 Td in NO^+ mode. Instrument backgrounds were
163 automatically measured during the last two minutes of each operation mode by passing
164 ambient air through a platinum catalyst heated to 365 °C. A gas standard containing 39
165 VOC species was used to calibrate the PTR-ToF-MS daily. Sensitivities for the
166 remaining species were determined based on reaction kinetics of the PTR-ToF-MS (*Wu*
167 *et al.*, 2020). Impacts of ambient humidity on the PTR-ToF-MS measurements were
168 corrected by using humidity-dependence curves of VOCs obtained in our laboratory
169 (*Wang et al.*, 2020a; *Wu et al.*, 2020). Carbon dioxide (CO_2 in dry air) and humidity
170 were measured using a CO_2 and H_2O gas analyzer (Li-840A, Licor Inc., USA) at a time
171 resolution of 10 seconds.

172 Gradient measurements of the total OH reactivity (OHR) of atmospheric trace
173 gases were made using the improved comparative reactivity method (ICRM) developed
174 by our team (*Wang et al.*, 2021a) from July 28 to 31. In addition, gradient measurements
175 of carbon monoxide (CO), methane (CH_4), CO_2 , and H_2O were simultaneously
176 measured using the cavity ring-down spectroscopy (CRDS) method (G-2401, Picarro
177 Inc., USA) at a time resolution of 10 seconds from May 15 to June 25. Sulfur dioxide
178 (SO_2) was measured using the ultraviolet fluorescence method (43i, Thermo Fisher
179 Scientific Inc., USA) at a time resolution of 10 seconds from June 25 to August 3. The
180 total OHR of VOCs, denoted by OHR_{VOCs} , can be estimated by excluding those of the
181 inorganic species (namely ozone, NO_x , CO, SO_2 , and CH_4). It should be noted that
182 gradient measurements of CH_4 and CO were not made during July 28-31, and their
183 average concentrations in daytime (11:00-16:00 LT) between May 15 and June 25 at 5
184 m were used for all altitudes to calculate OHR_{VOCs} . This method will bring minor
185 uncertainties due to the minor vertical differences in concentrations of CH_4 and CO in
186 daytime (Fig. S3S4). The OHR of VOCs can also be calculated by summing the
187 products of their measured concentrations and their reaction rate coefficients with OH
188 radicals, as formulated in Eq. (1):

$$\text{OHR} = \sum k^i_{\text{OH-R}}[\text{VOC}_i] \quad \text{Eq. (1)}$$

189 where $k^i_{\text{OH-R}}$ is the reaction rate coefficient of the i^{th} VOC species with OH radical
 190 and $[\text{VOC}_i]$ is the concentration of the i^{th} VOC species.

191 2.2 Estimation of NMHC concentrations at the BMT site

192 The PTR-ToF-MS is limited in its ability to measure VOC species with proton
 193 affinities higher than H₂O (691 kJ mol⁻¹) when operating in the H₃O⁺ mode (*Yuan et*
 194 *al., 2017*). This limitation results in the absence of certain nonmethane hydrocarbons
 195 (NMHCs), such as alkanes and many alkene species, which play important roles in
 196 photochemical ozone formation. To obtain a comprehensive understanding of vertical
 197 variations in concentrations, compositions, and environmental impacts of VOCs, this
 198 study estimated the vertical profiles of those unmeasured NMHC species based on the
 199 concentrations of measured VOCs using the PTR-ToF-MS. Detailed information on
 200 estimation of NMHC concentrations is provided in SI.

201 2.3 Box model setup

202 A zero-dimension box model (F0AM) coupled with the Master Chemical
 203 Mechanism (v3.3.1) (*Wolfe et al., 2016; Yang et al., 2022*) was used to compute the
 204 production rate of ozone, denoted by P(O₃) as formulated in Eq. (2):

$$P(\text{O}_3) = k_{\text{HO}_2+\text{NO}}[\text{HO}_2][\text{NO}] + \sum k^i_{\text{RO}_2+\text{NO}}[\text{R}^i\text{O}_2][\text{NO}] \quad \text{Eq. (2)}$$

$$205 \quad k_{\text{RO}_2+\text{NO}}[\text{RO}_2][\text{NO}]$$

206 where [HO₂] and [NO] is the concentrations of HO₂ and NO, [RⁱO₂] is the concentration
 207 of the i^{th} organic peroxy radical. The relative incremental reactivity (RIR) of
 208 photochemical ozone production to changes in different precursors was determined
 209 using Eq. (3):

$$\text{RIR}(X) = \frac{[P_{\text{O}_x}^S(X) - P_{\text{O}_x}^S(X - \Delta X)]/P_{\text{O}_x}^S(X)}{\Delta S(X)/S(X)} \quad \text{Eq. (3)}$$

210 where X represents ozone precursors, $P_{O_x}^S(X)$ is the contribution of X to the production
211 rate of O_x , ΔX is the amount of change in ozone precursors, $S(X)$ is the initial
212 concentration of X. RIR values were used to discern sensitivities of photochemical
213 ozone formation to changes in precursor gases. A positive RIR(X) value suggests that
214 an increase in X enhances ozone formation, while a negative RIR value indicates that
215 an increase in X inhibits ozone formation.

216 Model calculations were constrained by measurements of ozone, NO_x , CO, a suit
217 of VOCs, air temperature, and relative humidity. In addition to the measured or
218 estimated concentrations of NMHCs, nine oxygenated VOC (OVOC) species (Table
219 S1) measured by PTR-ToF-MS were used to constrain the model calculation. The
220 model was run in a time-dependent mode with a time resolution of 5 minutes and a
221 spin-up period of 2 days (Lu et al., 2012; Wang et al., 2022c). The dry deposition
222 velocity of ozone was set as 0.27 cm s^{-1} when calculating $P(O_3)$ 5 m and was zeroed
223 out when calculating $P(O_3)$ at other heights.

224 **3 Results and discussions**

225 **3.1 Temporal and vertical variations in concentrations of trace gases**

226 As shown in Fig. 1, the meteorology in Beijing was characterized by high air
227 temperature ($27.3 \pm 2.9 \text{ }^\circ\text{C}$), high humidity ($83.9\% \pm 16.2\%$), and gentle winds (1.1 ± 0.4
228 m s^{-1}) throughout the campaign. The intense solar radiation, elevated air temperature,
229 and mild winds favored the photochemical formation and accumulation of ozone,
230 leading to frequent occurrences of ozone pollution episodes. Fig. 1 also presents time
231 series of mixing ratios of ozone and its selected precursors (namely isoprene, toluene,
232 monoterpenes, and NO_x) along with $j(NO_2)$ measured at 5 m. The campaign mean
233 ozone mixing ratio was $45.6 \pm 25.3 \text{ ppb}$, but the maximum hourly mean ozone mixing
234 ratio reached 129.3 ppb , indicating strong photochemical reactions in urban Beijing
235 during the campaign. Surface ozone concentrations exhibited a typical diurnal variation

236 pattern with the maximum occurring at 16:00 LT (Fig. S5S6), implying its predominant
237 source from local photochemical production.

238 Isoprene is a typical tracer of biogenic emissions and is also a highly reactive VOC
239 species (Atkinson and Arey, 2003). Isoprene had a campaign mean mixing ratio of
240 0.7 ± 0.6 ppb. The average diurnal profile of isoprene at 5 m has a unimodal pattern with
241 the maximum occurring at 14:00 LT (Fig. S5S6), exhibiting strong dependence on solar
242 radiation. Monoterpenes were also generally recognized as typical tracers of biogenic
243 emissions (Gómez et al., 2020) and have a campaign mean mixing ratio of 0.3 ± 0.3 ppb.
244 The average diurnal profile of monoterpenes was characterized by low mixing ratios in
245 daytime with two peaks occurring at 05:00 and 20:00 LT, respectively.

246 Toluene and NO_x are recognized as typical tracers of anthropogenic emissions in
247 urban regions (Niu et al., 2017; Li et al., 2022c), with campaign mean mixing ratios of
248 0.7 ± 0.7 and 8.1 ± 4.8 ppb, respectively. The average diurnal profiles of toluene and NO_x
249 at 5 m exhibited similar variations with larger values at night than during the day. Based
250 on the measured concentrations and diurnal variations of ozone and its key precursors
251 at ground level, it can be inferred that urban Beijing is experiencing severe ozone
252 pollution, which is predominantly contributed by local photochemical production. As
253 key ozone precursors, ambient concentrations of VOCs are contributed by the mixture
254 of anthropogenic and biogenic sources.

255 Fig. 2 shows the average diurnal and vertical variations in mixing ratios of ozone,
256 NO_x, Ox (O₃+NO₂), and six selected VOC species (three hydrocarbons and three
257 OVOCs) within the measurement height range of 5-320 m. High mixing ratios of ozone
258 were observed in the afternoon following the enhancement of solar radiation, which
259 was consistent with the diurnal change pattern of ozone concentrations at the ground
260 level. The vertical gradients of ozone mixing ratios were positive throughout the day
261 but substantially enhanced at night (Fig. 3). The lower ozone mixing ratios near the
262 surface than aloft were mainly caused by the enhancement of dry deposition and NO
263 titration (Brown et al., 2007; Ma et al., 2013; Li et al., 2022b).

264 NO_x is a primary pollutant and mainly contributed by vehicular exhausts in urban
265 regions. In contrast to ozone, NO_x mixing ratios were low in daytime and exhibited
266 negative vertical gradients throughout the day, as shown in Figs. 2B and 3A-B. In
267 nighttime, large amounts of local NO_x emissions were trapped and accumulated in a
268 shallow boundary layer (<100 m). NO_x concentrations rapidly decreased with height
269 even in the overlying residual layer due to the suppression of turbulence vertical mixing.
270 With the onset of sunlight, the PBL rapidly expanded due to the surface heating effect.
271 The accumulated high concentrations of NO_x in the shallow nocturnal boundary layer
272 were thereupon diluted and removed by photochemical reactions.

273 Ox is frequently used as a conserved metric to investigate temporal and spatial
274 variability of ozone by eliminating the NO titration effect. As shown in Fig. 2C, the
275 mixing ratios of Ox had similar diurnal and vertical variation patterns to those of ozone,
276 but the vertical gradients of Ox were weaker than those of ozone. This result suggests
277 that the vertical distribution of NO concentrations played an important role in regulating
278 the vertical change of ozone concentrations. The enhanced positive gradients of ozone
279 mixing ratios at night were predominantly due to the strict suppression of turbulence
280 vertical mixing (*Geyer and Stutz, 2004*). The higher concentrations of ozone aloft are
281 considered as the residual of the ozone produced in the daytime PBL and have been
282 recognized as an important reservoir for the enhancement of surface ozone in morning
283 periods (*Kaser et al., 2017; Li and Fan, 2022; He et al., 2023*).

284 Benzene and toluene demonstrated similar diurnal and vertical variations to NO_x,
285 with low concentrations in daytime and high concentrations at night, as shown in Figs.
286 2D-F and 3A-B. The concentrations of both benzene and toluene decreased with height
287 throughout the day, confirming their primary emissions from ground-level sources.
288 However, unlike benzene, the diurnal and vertical variations of toluene were more
289 pronounced. Isoprene emissions are highly dependent on solar radiation, resulting in its
290 higher concentrations in the early afternoon compared to other times of the day.
291 Isoprene mixing ratios also exhibited strong negative vertical gradients below 320 m
292 throughout the day. In contrast to toluene, isoprene concentrations decreased more

293 rapidly with height in the daytime. For instance, the mixing ratios of isoprene decreased
294 by approximately 70% from 5 to 320 m in the daytime, while it was only 30% for
295 toluene.

296 Fig. 3A-B show the average vertical profiles of the NMHCs, normalized to their
297 respective ground-level concentrations measured by the PTR-ToF-MS in daytime and
298 nighttime. The normalized mixing ratios of the NMHCs exhibited significantly
299 differentiated gradients in daytime. In contrast, apart from monoterpenes, the
300 differences in vertical gradients of the normalized vertical profiles for other NMHCs
301 were relatively small at night. The differentiated vertical gradients of the NMHCs in
302 daytime were primarily caused by their intrinsic chemical reactivities, such as reactions
303 with OH radicals. As shown in Fig. 4, concentration ratios of the NMHC species
304 between 320 m and 5 m with k_{OH} values lower than $2.5 \times 10^{-11} \text{ cm}^3 \text{ molecule}^{-1} \text{ s}^{-1}$
305 exhibited slight variability and rapidly declined with the further increases in k_{OH} . The
306 lower NMHC concentrations at higher altitudes were predominantly caused by the
307 combined effects of atmospheric diffusion and chemical removal (*Sangiorgi et al.*,
308 2011).

309 Considering the effects of atmospheric diffusion and chemical removal by
310 reactions with OH radicals, concentration ratios of NMHC species between 320 m and
311 5 m in daytime can be estimated using Eq. (4):

$$y = A \times \exp(-k_{OH}[\text{OH}]\Delta t) \quad \text{Eq. (4)}$$

312 where y represents concentration ratios of the NMHC species between two altitudes, A
313 represents the effect of atmospheric dilution, k_{OH} is the reaction rate coefficient of
314 NMHCs with OH radicals, $[\text{OH}]$ is the concentration of OH radical, Δt is the
315 turbulence mixing time scale between the two altitudes. The term $[\text{OH}]\Delta t$ thus refers
316 to the exposure of NMHCs to OH radicals between the two altitudes. As shown in Fig.
317 4, the average concentration ratios of NMHCs between 320 m and 5 m in daytime
318 during the campaign can be well reproduced using Eq. (4) with the coefficients A of
319 0.88 and $[\text{OH}]\Delta t$ of $1.0 \times 10^{10} \text{ molecules cm}^{-3} \text{ s}$. Atmospheric diffusion processes have
320 same impact on the vertical distributions of all trace gases. The differences in vertical

321 gradients of NMHCs were mainly determined by the differences in their chemical
322 removal rates without considering influences from advection transport.

323 Methanol, as one of the most abundant OVOC species in the atmosphere, had its
324 lowest concentrations during daytime and displayed negative vertical gradients
325 throughout the day, as shown in Fig. 2G. The vertical and diurnal variations of methanol
326 suggest that its ambient concentrations in urban Beijing were mainly contributed by
327 local primary emissions. Conversely, formaldehyde and MVK+MACR (the first-
328 generation oxidation products of isoprene), as the photochemical oxidation products of
329 NMHCs, had higher concentrations during daytime than at night and exhibited
330 relatively weak vertical concentration gradients (Fig. 2H-I). This is mainly because
331 these OVOCs are produced from the oxidation of NMHCs during turbulence vertical
332 mixing and will accumulate in high altitudes. These phenomena were also observed for
333 other OVOC species, as shown in Fig. 3.

334 The vertical and diurnal variations in concentrations of ozone, NO_x, and VOCs
335 are intricately governed by their sources, chemical reactivities, and the evolution of the
336 PBL (namely the vertical dilution conditions). A significant accumulation of VOCs in
337 the shallow nocturnal PBL is subsequently vertically diluted and chemically removed
338 during daytime, thereby impacting the photochemical formation of ozone within the
339 daytime PBL. In addition, the observed vertical changes in concentrations of VOCs
340 imply that they will play distinct roles in contributing to photochemical ozone
341 formation.

342 **3.2 Vertical variations in contributions of VOCs to OHR**

343 During the daytime, VOCs are primarily oxidized by OH radicals and contribute
344 to the photochemical formation of ozone. To provide an overview on the vertical
345 variations in contributions of different VOCs to OHR, another 1204 ions measured by
346 the PTR-ToF-MS and can be quantified were used for analysis. All the VOCs were
347 classified into three large categories, namely C_xH_y (including alkanes, alkenes,
348 aromatics, and other hydrocarbons; 121 species), OVOCs (C_xH_yO₁, 121 species;

349 $C_xH_yO_2$, 120 species; $C_xH_yO_{\geq 3}$, 256 species), and N/S-containing (653 species), as
350 shown in Fig.5. Acetylene is included in alkenes.

351 Fig. 5A illustrates that the total mixing ratios of VOCs in daytime exhibited a slight
352 downward trend from 5 m to 320 m, primarily due to the rapid decrease in mixing ratios
353 of the C_xH_y category. The total mixing ratios of the C_xH_y category decreased from 16.8
354 to 10.6 ppb from 5 m to 320 m, with alkanes making the largest contribution, followed
355 by alkenes, aromatics, and other C_xH_y . Alkanes constituted 58% of the total mixing
356 ratios of C_xH_y at 5 m, but this proportion increased to 65% at 320 m. The fractional
357 contributions of alkenes and aromatics in the total mixing ratios of C_xH_y slightly
358 declined from 28% to 22% and from 12% to 10%, respectively, between these two
359 altitudes. As for OVOCs, the $C_xH_yO_1$ category was the most abundant among the
360 measurements, contributing to 52%-58% of the total mixing ratios at the five heights,
361 followed by the $C_xH_yO_2$ (8%-10%), and $C_xH_yO_{\geq 3}$ (2%) categories. The mixing ratios of
362 the N/S-containing category slightly varied around 2.8 ppb between 5-320 m,
363 contributed to approximately 6% of the total VOC concentrations.

364 Similar to the vertical variations in concentrations, OHRs of the C_xH_y category,
365 denoted by OHR_{CH} , also rapidly decreased from 6.9 s^{-1} to 2.5 s^{-1} between 5 and 320 m,
366 accounting for 52%-31% in the total OHRs of VOCs (Fig. 5B). Fractional contributions
367 of alkenes (40-18%), alkanes (5%), and aromatics (5%-4%) to the total OHRs of VOCs
368 all exhibited decreasing tendencies from 5 m to 320 m. The total OHRs of alkenes
369 decreased more quickly from 5 to 320 m than those of alkanes and aromatics. OHRs of
370 the other C_xH_y category stabilized at approximately 0.3 s^{-1} below 320 m, exhibiting an
371 increasing contribution (2%-4%) to the total OHRs of VOCs with the increase in height.
372 The OHRs of other VOC categories only slightly varied without exhibiting a clear
373 variation trend from 5 to 320 m during the day. As a result, fractional contributions of
374 the $C_xH_yO_1$ (27%-42%), $C_xH_yO_2$ (12%-18%), and $C_xH_yO_{\geq 3}$ (5%-7%), and N/S-
375 containing (2%-4%) categories in the total OHRs of VOCs all increased with height.
376 The increased contributions of OVOCs and N/S-containing species to the total

377 concentrations and OHRs of VOCs implied that air masses became more aged with the
378 increase in height.

379 As depicted in Fig. 6A-B, high OHR_{CH} values were mainly constrained in the PBL
380 and is mainly contributed by biogenic hydrocarbons, specifically isoprene, during
381 daytime due to their high OH reactivities and enhanced emissions. The fractional
382 contributions of isoprene in OHR_{CH} decreased rapidly with increasing height (Fig. 7A).
383 For instance, isoprene accounted for a campaign median fraction of 58% in OHR_{CH} at
384 5 m in daytime, making it a frequent contributor to photochemical ozone formation in
385 urban regions. However, this fraction decreased to 38% at 320 m. Therefore, it can be
386 speculated that the total contributions of hydrocarbons to the total OHRs of VOCs will
387 also rapidly decline from 320 m to the top of the PBL, which typically ranges between
388 several hundreds of meters to approximately 2~3 km in daytime (Fig. S6S7).

389 The total concentrations and OHRs of OVOCs only slightly decreased with the
390 increase in height below 320 m in daytime, as shown in Fig. 6C-D. This is consistent
391 with the results of (Wang *et al.*, 2021b), which observed high concentrations of OVOCs
392 in the upper PBL. Consequently, the ratio of OHR_{OVOC} to OHR_{CH} , denoted by
393 $\text{OHR}_{\text{OVOC}}/\text{OHR}_{\text{CH}}$, rapidly increased from 0.87 at 5 m to 2.6 at 320 m (Fig. 7A). This
394 suggests that OVOCs may play more important roles in regulating the photochemical
395 ozone formation in the middle and upper layers. To assess their potential roles in
396 contributing to the photochemical ozone formation throughout the PBL, we calculated
397 the mean OHRs (MOHR) of different VOC categories in daytime using Eq. (5):

$$\text{MOHR}(X) = \left(\sum ([X]_i + [X]_{i-1})(h_i - h_{i-1})/2 \right) / (320 - 5) \quad \text{Eq. (5)}$$

398 where $\text{MOHR}(X)$ is the MOHR of the VOC category X, $[X]_i$ is the concentration of
399 X at the i^{th} altitude (namely 5, 47, 102, 200, and 320 m for h_i) above ground level.

400 As shown in Fig. 7B, the campaign median MOHR for isoprene was 1.7 s^{-1} and
401 accounted for 48% of the campaign median MOHR of the C_xH_y category. This fraction
402 was significantly lower than that of isoprene (57%) in OHR_{CH} at 5 m. In addition, the
403 campaign median MOHR of the C_xH_y category (3.5 s^{-1}) was also significantly lower

404 than the OHR_{CH} (6.0 s^{-1}) at 5 m. By contrast, the campaign median MOHR of OVOCs
405 (4.8 s^{-1}) was comparable to that of OHR_{OVOC} (4.9 s^{-1}) at 5 m. As unsaturated
406 hydrocarbons, most alkene species are more reactive than alkanes and aromatics
407 (*Atkinson and Arey, 2003*). As a result, alkenes had dominant contributions to the
408 MOHR of the C_xH_y category and the OHR_{CH} at 5 m in daytime. As shown in Fig. 7C,
409 the campaign mean OHRs of alkanes, alkenes, and aromatics at 5 m in daytime were
410 0.7 , 5.2 , and 0.7 s^{-1} , respectively, accounting for 10%, 75%, and 10% of the OHR_{CH} .
411 However, the campaign mean MOHRs of alkanes, alkenes, and aromatics were 0.5 , 2.7 ,
412 and 0.5 s^{-1} , respectively, accounting for 12%, 68%, and 12% of the MOHR of NMHC.
413 We can also expect that the total contributions of alkenes to the MOHR of the C_xH_y
414 category in daytime will significantly decrease if their vertical distributions in the whole
415 PBL are considered.

416 This study investigated and compared the vertical profiles of measured OHR_{VOCs}
417 and calculated OHR_{CH} during daytime over the period of July 28-31, as shown in Fig.
418 7D. The campaign median of the measured OHR_{VOCs} exhibited a slow decrease from
419 38.4 s^{-1} at 5 m to 25.4 s^{-1} at 320 m. As anticipated, the $\text{OHR}_{\text{CH}}/\text{OHR}_{\text{VOCs}}$ ratio declined
420 rapidly from 16% to 7% from 5 to 320 m. It is important to note that the small
421 $\text{OHR}_{\text{CH}}/\text{OHR}_{\text{VOCs}}$ ratio and its declining trend with the increasing height do not imply
422 the insignificant roles of hydrocarbons in regulating the secondary pollutant formation
423 in higher altitudes. The measured concentrations of hydrocarbons are merely the
424 remnants of chemical reactions. The oxidation products of NMHCs, such as OVOCs
425 and organic nitrates, formed during vertical mixing in daytime, will continue to
426 participate in atmospheric chemical reactions.

427 **3.3 Vertical variations in photochemical ozone formation**

428 The surface ozone budget is intimately linked to the vertical variations of
429 photochemical ozone formation throughout the PBL. Previous studies have consistently
430 reported that the photochemical formation of ozone, encompassing both $\text{P}(\text{O}_3)$ and
431 ozone formation regimes (namely the NO_x -limited, VOCs-limited, and transition

432 regimes), are highly dependent on the change in its precursors (*Shao et al., 2021; Yang*
433 *et al., 2022*). Consequently, any changes in the concentrations and compositions of
434 VOCs and NO_x within the PBL will inevitably lead to alternations in the vertical
435 distribution of P(O₃) and ozone formation regimes (*Tang et al., 2017; Li et al., 2024*).

436 Fig. 8A illustrates the average dependence of P(O₃) on NO_x concentrations along
437 with the normalized probability density (NPD) distribution of NO_x concentrations at 5
438 m, 200 m, and 320 m in daytime during the field campaign. At different heights, P(O₃)
439 all rapidly increased with the rise in NO_x until a critical NO_x mixing ratio was reached,
440 after which P(O₃) decreased slowly. The critical NO_x mixing ratios decreased from
441 approximately 9.5 ppb at 5 m to 5.0 ~~ppb~~ ppb at 320 m, primarily caused by the decreases
442 in both NO_x concentrations and the OHRs of VOCs. As also shown in Fig. 8A, the
443 majority of the measured NO_x mixing ratios fall into the transition zone of the P(O₃)-
444 NO_x curves, suggesting that the photochemical ozone formation in Beijing belonged to
445 the transition regime below 320 m.

446 RIR values were also calculated using the box model results to further elucidate
447 the sensitivities of photochemical ozone formation to changes in multiple precursors at
448 different altitudes. As shown in Fig. 8B, positive RIR values were observed for both
449 NO_x and various VOC groups at the five heights, further confirming that the
450 photochemical ozone formation belonged to the transition regime in the lower layer.
451 RIR values for NO_x rapidly declined from 5 to 320 m, implying that the photochemical
452 ozone formation in higher altitudes ~~were~~ was more prone to be controlled by the
453 abundance of VOCs. This is also manifested by the increasing RIR values for both
454 AVOCs and OVOCs from 5 m to 320 m. RIR values for BVOCs significantly decreased
455 with height due to their rapid removal by reactions with OH radicals when being
456 vertically mixed. These results are consistent with the results in section 3.3 that the less
457 reactive AVOCs and OVOCs are the dominant species in regulating the photochemical
458 formation of ozone in urban regions aloft.

459 According to the vertical distribution patterns of the photochemical ozone
460 formation regime, P(O₃) decreases with increasing height alongside simultaneous

461 declines in concentrations of both NO_x and VOCs. Fig. 8C presents the average diurnal
462 and vertical variations in $P(\text{O}_3)$ calculated by the box model during the campaign. The
463 $P(\text{O}_3)$ values were higher in daytime and correlated well with $j(\text{NO}_2)$. ~~As shown in Fig.~~
464 ~~S7, OH radical concentrations and $P(\text{O}_3)$ exhibited contrasting vertical distribution~~
465 ~~patterns in daytime.~~ $P(\text{O}_3)$ decreased from the ground to 320 m, where it still maintained
466 a relatively high value of approximately 10 ppb h⁻¹ at noon. These results highlight that
467 the photochemical formation of ozone aloft also remained strong compared to those at
468 ground level. Consequently, the downward transport of ozone from high altitudes,
469 driven by turbulence mixing, can become significant sources of surface ozone during
470 the day (Karl et al., 2023).

471 Due to the measurement height limitation, the vertical distributions of $P(\text{O}_3)$ in the
472 middle and upper parts of the PBL were not determined in this study. As reported by
473 the work in (Benish et al., 2020), $P(\text{O}_3)$ typically exhibited weak and nearly linear
474 decline tendencies from 300 m to the top of the PBL during daytime. $P(\text{O}_3)$ at the PBL
475 top was approximately half of that at 300 m. Consequently, we can assume that $P(\text{O}_3)$
476 decreased linearly from 320 m to the top of the PBL. The integral of $P(\text{O}_3)$ at different
477 heights within the PBL can then be estimated using a similar method as described in
478 Eq. (5).

479 As shown in Fig. 8D, the total amount of ozone photochemically produced below
480 47 m constituted a mere 6% of the entire PBL. This fractional contribution increased to
481 approximately 35% at 320 m, further corroborating that the majority of the boundary-
482 layer ozone was produced in the middle and upper layers. Given the enhancement of
483 turbulence vertical mixing in daytime, ozone produced at high altitudes becomes a
484 significant source of surface ozone. This is substantiated by the widespread reports of
485 strong downward ozone fluxes in the bottom part of the PBL (tens of meters above
486 ground level) (Fares et al., 2010; Liu et al., 2021; Karl et al., 2023). Consequently,
487 when devising ozone control strategies, particularly in urban regions with intricate
488 precursor emissions, careful considerations should be given to the vertical variations in
489 the formation regimes of ozone in the PBL.

490 **4 Conclusions**

491 In this study, we investigated the vertical variations, key drivers, and
492 environmental impacts of VOCs in the PBL using tower-based online gradient
493 measurements in urban Beijing during the summer of 2021. The diurnal and vertical
494 variations of various VOC species were strictly regulated by the diurnal evolution of
495 the PBL. In daytime, reactive NMHC species were rapidly oxidized when they were
496 mixed upward along with the formation of OVOCs. As a result, OVOC species played
497 more significant roles in regulating the photochemical ozone formation in urban regions
498 aloft. The photochemical formation of ozone belongs to the transition regime in the
499 lower part of the PBL and becomes more sensitive to changes in the concentrations of
500 AVOCs and OVOCs with increasing height. $P(O_3)$ exhibited decreasing tendencies
501 with height but remained very large in high altitudes, likely driven by the high
502 concentrations of OVOCs and OH radicals. Therefore, careful consideration should be
503 given to the vertical variations in both $P(O_3)$ and photochemical ozone formation
504 regimes in the whole PBL when making regional ozone control strategies.

505 The vertical variations in concentrations and compositions of VOCs significantly
506 influence the formation of secondary pollutants. Furthermore, vertical changes in
507 chemical reaction environments (e.g., temperature, humidity, and solar radiation) and
508 concentrations of other chemicals (e.g., particulate matters, NO_x , ozone) can also
509 impact the degradation pathways of VOCs. These factors also affect the formation
510 pathways and production yields of secondary pollutants. This is particularly crucial for
511 the highly reactive NMHCs in urban areas with complex anthropogenic emissions and
512 is expected to be thoroughly elucidated in future studies.

513 **Data availability**

514 The observational data used in this study are available from corresponding authors
515 upon request.

516 **Author contributions**

517 BY, XBL, and YH designed the research. XBL, BY, YH, XS, JQ, XH, SW, YC,
518 QY, YS, YP, GT, JG, and MS contributed to the data collection and data analysis. XBL,
519 SY, and BY designed and performed the box model simulations. XBL and BY wrote
520 the paper with contributions from all coauthors. All the coauthors discussed the results
521 and reviewed the paper.

522 **Competing interests**

523 The authors declare that they have no conflict of interest.

524 **Acknowledgments**

525 The authors would like to thank the personnel who participated in data collection,
526 instrument maintenance, and logistic support during the field campaign.

527 **Financial support**

528 This work was financially supported by the National Key R&D Plan of China
529 (grant nos. 2023YFC3706103, 2023YFC3706201, 2023YFC3710900, and
530 2022YFC3700604) and the National Natural Science Foundation of China (grant nos.
531 42121004, 42275103, 42205094, 42230701, ~~and~~42305095, ~~and~~42475107). This work
532 was also supported by the Guangdong Basic and Applied Basic Research Foundation
533 (grant no. 2024A1515011570) and Guangzhou Basic and Applied Basic Research
534 Foundation (grant no. 2024A04J3958).

535 **References**

536 An, J., Huang, Y., Huang, C., Wang, X., Yan, R., Wang, Q., Wang, H., Jing, S., Zhang,
537 Y., Liu, Y., Chen, Y., Xu, C., Qiao, L., Zhou, M., Zhu, S., Hu, Q., Lu, J., and Chen, C.:
538 Emission inventory of air pollutants and chemical speciation for specific anthropogenic
539 sources based on local measurements in the Yangtze River Delta region, China, *Atmos.*
540 *Chem. Phys.*, 21, 2003-2025, <https://doi.org/10.5194/acp-21-2003-2021> 2021.
541 Atkinson, R., and Arey, J.: Atmospheric Degradation of Volatile Organic Compounds,
542 *Chem Rev*, 103, 4605-4638, <https://doi.org/10.1021/cr0206420> 2003.

543 Benish, S. E., He, H., Ren, X., Roberts, S. J., Salawitch, R. J., Li, Z., Wang, F., Wang,
544 Y., Zhang, F., Shao, M., Lu, S., and Dickerson, R. R.: Measurement report: Aircraft
545 observations of ozone, nitrogen oxides, and volatile organic compounds over Hebei
546 Province, China, *Atmos. Chem. Phys.*, 20, 14523-14545,[https://doi.org/10.5194/acp-](https://doi.org/10.5194/acp-20-14523-2020)
547 [20-14523-2020](https://doi.org/10.5194/acp-20-14523-2020) 2020.

548 Brown, S. S., Dubé, W. P., Osthoff, H. D., Wolfe, D. E., Angevine, W. M., and
549 Ravishankara, A. R.: High resolution vertical distributions of NO₃ and N₂O₅ through
550 the nocturnal boundary layer, *Atmos. Chem. Phys.*, 7, 139-149,[10.5194/acp-7-139-](https://doi.org/10.5194/acp-7-139-2007)
551 [2007](https://doi.org/10.5194/acp-7-139-2007) 2007.

552 Cooper, O. R., Schultz, M. G., Schroeder, S., Chang, K.-L., Gaudel, A., Benitez, G. C.,
553 Cuevas, E., Froehlich, M., Galbally, I. E., Molloy, S., Kubistin, D., Lu, X., McClure-
554 Begley, A., Nedelec, P., O'Brien, J., Oltmans, S. J., Petropavlovskikh, I., Ries, L., Senik,
555 I., Sjoeborg, K., Solberg, S., Spain, G. T., Spangl, W., Steinbacher, M., Tarasick, D.,
556 Thouret, V., and Xu, X.: Multi-decadal surface ozone trends at globally distributed
557 remote locations, *Elementa-Science of the Anthropocene*,
558 8,<https://doi.org/10.1525/elementa.420> 2020.

559 Dieu Hien, V. T., Lin, C., Thanh, V. C., Kim Oanh, N. T., Thanh, B. X., Weng, C.-E.,
560 Yuan, C.-S., and Rene, E. R.: An overview of the development of vertical sampling
561 technologies for ambient volatile organic compounds (VOCs), *J Environ Manage*, 247,
562 401-412,<https://doi.org/10.1016/j.jenvman.2019.06.090> 2019.

563 Fares, S., McKay, M., Holzinger, R., and Goldstein, A. H.: Ozone fluxes in a *Pinus*
564 *ponderosa* ecosystem are dominated by non-stomatal processes: Evidence from long-
565 term continuous measurements, *Agr Forest Meteorol*, 150, 420-
566 431,<https://doi.org/10.1016/j.agrformet.2010.01.007> 2010.

567 Fleming, Z. L., Doherty, R. M., von Schneidmesser, E., Malley, C. S., Cooper, O. R.,
568 Pinto, J. P., Colette, A., Xu, X., Simpson, D., Schultz, M. G., Lefohn, A. S., Hamad, S.,
569 Moolla, R., Solberg, S., and Feng, Z.: Tropospheric Ozone Assessment Report: Present-
570 day ozone distribution and trends relevant to human health, *Elementa-Science of the*
571 *Anthropocene*, 6,[10.1525/elementa.273](https://doi.org/10.1525/elementa.273) 2018.

572 Geng, C., Wang, J., Yin, B., Zhao, R., Li, P., Yang, W., Xiao, Z., Li, S., Li, K., and Bai,
573 Z.: Vertical distribution of volatile organic compounds conducted by tethered balloon
574 in the Beijing-Tianjin-Hebei region of China, *Journal of Environmental Sciences*, 95,
575 121-129,<https://doi.org/10.1016/j.jes.2020.03.026> 2020.

576 Geyer, A., and Stutz, J.: Vertical profiles of NO₃, N₂O₅, O₃, and NO_x in the nocturnal
577 boundary layer: 2. Model studies on the altitude dependence of composition and
578 chemistry, *Journal of Geophysical Research: Atmospheres*,
579 109,<https://doi.org/10.1029/2003jd004211> 2004.

580 Gkatzelis, G. I., Coggon, M. M., McDonald, B. C., Peischl, J., Gilman, J. B., Aikin, K.
581 C., Robinson, M. A., Canonaco, F., Prevot, A. S. H., Trainer, M., and Warneke, C.:
582 Observations Confirm that Volatile Chemical Products Are a Major Source of
583 Petrochemical Emissions in U.S. Cities, *Environ Sci Technol*, 55, 4332-
584 4343,[10.1021/acs.est.0c05471](https://doi.org/10.1021/acs.est.0c05471) 2021.

585 Gómez, M. C., Durana, N., García, J. A., de Blas, M., Sáez de Cámara, E., García-Ruiz,
586 E., Gangoiti, G., Torre-Pascual, E., and Iza, J.: Long-term measurement of biogenic

587 volatile organic compounds in a rural background area: Contribution to ozone
588 formation, *Atmos Environ*, 224,
589 117315,<https://doi.org/10.1016/j.atmosenv.2020.117315> 2020.

590 Guo, H., Ling, Z. H., Cheng, H. R., Simpson, I. J., Lyu, X. P., Wang, X. M., Shao, M.,
591 Lu, H. X., Ayoko, G., Zhang, Y. L., Saunders, S. M., Lam, S. H. M., Wang, J. L., and
592 Blake, D. R.: Tropospheric volatile organic compounds in China, *Sci Total Environ*,
593 574, 1021-1043,<https://doi.org/10.1016/j.scitotenv.2016.09.116> 2017.

594 Guo, J.-X., Zeng, Y., Zhu, K., and Tan, X.: Vehicle mix evaluation in Beijing's
595 passenger-car sector: From air pollution control perspective, *Sci Total Environ*, 785,
596 147264,<https://doi.org/10.1016/j.scitotenv.2021.147264> 2021.

597 He, G., He, C., Wang, H., Lu, X., Pei, C., Qiu, X., Liu, C., Wang, Y., Liu, N., Zhang,
598 J., Lei, L., Liu, Y., Wang, H., Deng, T., Fan, Q., and Fan, S.: Nighttime ozone in the
599 lower boundary layer: insights from 3-year tower-based measurements in South China
600 and regional air quality modeling, *Atmos. Chem. Phys.*, 23, 13107-13124,[10.5194/acp-](https://doi.org/10.5194/acp-23-13107-2023)
601 [23-13107-2023](https://doi.org/10.5194/acp-23-13107-2023) 2023.

602 He, X., Yuan, B., Wu, C., Wang, S., Wang, C., Huangfu, Y., Qi, J., Ma, N., Xu, W.,
603 Wang, M., Chen, W., Su, H., Cheng, Y., and Shao, M.: Volatile organic compounds in
604 wintertime North China Plain: Insights from measurements of proton transfer reaction
605 time-of-flight mass spectrometer (PTR-ToF-MS), *J Environ Sci (China)*, 114, 98-
606 114,[10.1016/j.jes.2021.08.010](https://doi.org/10.1016/j.jes.2021.08.010) 2022.

607 Hofzumahaus, A., Rohrer, F., Lu, K., Bohn, B., Brauers, T., Chang, C.-C., Fuchs, H.,
608 Holland, F., Kita, K., Kondo, Y., Li, X., Lou, S., Shao, M., Zeng, L., Wahner, A., and
609 Zhang, Y.: Amplified Trace Gas Removal in the Troposphere, *Science*, 324, 1702-
610 1704,[doi:10.1126/science.1164566](https://doi.org/10.1126/science.1164566) 2009.

611 Karl, T., Lamprecht, C., Graus, M., Cede, A., Tiefengraber, M., Vila-Guerau de
612 Arellano, J., Gurarie, D., and Lenschow, D.: High urban NO_x triggers a substantial
613 chemical downward flux of ozone, *Science Advances*, 9,
614 eadd2365,[doi:10.1126/sciadv.add2365](https://doi.org/10.1126/sciadv.add2365) 2023.

615 Kaser, L., Patton, E. G., Pfister, G. G., Weinheimer, A. J., Montzka, D. D., Flocke, F.,
616 Thompson, A. M., Stauffer, R. M., and Halliday, H. S.: The effect of entrainment
617 through atmospheric boundary layer growth on observed and modeled surface ozone in
618 the Colorado Front Range, *Journal of Geophysical Research: Atmospheres*, 122, 6075-
619 6093,[10.1002/2016jd026245](https://doi.org/10.1002/2016jd026245) 2017.

620 Kim, S., Seco, R., Gu, D., Sanchez, D., Jeong, D., Guenther, A. B., Lee, Y., Mak, J. E.,
621 Su, L., Kim, D. B., Lee, Y., Ahn, J.-Y., McGee, T., Sullivan, J., Long, R., Brune, W.
622 H., Thames, A., Wisthaler, A., Mueller, M., Mikoviny, T., Weinheimer, A., Yang, M.,
623 Woo, J.-H., Kim, S., and Park, H.: The role of a suburban forest in controlling vertical
624 trace gas and OH reactivity distributions - a case study for the Seoul metropolitan area,
625 *Faraday Discuss*, 226, 537-550,[10.1039/d0fd00081g](https://doi.org/10.1039/d0fd00081g) 2021.

626 Li, C., Liu, Y., Cheng, B., Zhang, Y., Liu, X., Qu, Y., An, J., Kong, L., Zhang, Y.,
627 Zhang, C., Tan, Q., and Feng, M.: A comprehensive investigation on volatile organic
628 compounds (VOCs) in 2018 in Beijing, China: Characteristics, sources and behaviours
629 in response to O₃ formation, *Sci Total Environ*, 806,
630 150247,<https://doi.org/10.1016/j.scitotenv.2021.150247> 2022a.

631 Li, X.-B., Wang, D., Lu, Q.-C., Peng, Z.-R., Fu, Q., Hu, X.-M., Huo, J., Xiu, G., Li, B.,
632 Li, C., Wang, D.-S., and Wang, H.: Three-dimensional analysis of ozone and PM_{2.5}
633 distributions obtained by observations of tethered balloon and unmanned aerial vehicle
634 in Shanghai, China, *Stoch Env Res Risk A*, 32, 1189-
635 1203,<https://doi.org/10.1007/s00477-018-1524-2> 2018.

636 Li, X.-B., and Fan, G.: Interannual variations, sources, and health impacts of the
637 springtime ozone in Shanghai, *Environ Pollut*, 306,
638 119458,<https://doi.org/10.1016/j.envpol.2022.119458> 2022.

639 Li, X.-B., Yuan, B., Parrish, D. D., Chen, D., Song, Y., Yang, S., Liu, Z., and Shao, M.:
640 Long-term trend of ozone in southern China reveals future mitigation strategy for air
641 pollution, *Atmos Environ*, 269, 118869,[10.1016/j.atmosenv.2021.118869](https://doi.org/10.1016/j.atmosenv.2021.118869) 2022b.

642 Li, X.-B., Yuan, B., Wang, S., Wang, C., Lan, J., Liu, Z., Song, Y., He, X., Huangfu,
643 Y., Pei, C., Cheng, P., Yang, S., Qi, J., Wu, C., Huang, S., You, Y., Chang, M., Zheng,
644 H., Yang, W., Wang, X., and Shao, M.: Variations and sources of volatile organic
645 compounds (VOCs) in urban region: insights from measurements on a tall tower,
646 *Atmos. Chem. Phys.*, 22, 10567-10587,[10.5194/acp-22-10567-2022](https://doi.org/10.5194/acp-22-10567-2022) 2022c.

647 Li, X.-B., Zhang, C., Liu, A., Yuan, B., Yang, H., Liu, C., Wang, S., Huangfu, Y., Qi,
648 J., Liu, Z., He, X., Song, X., Chen, Y., Peng, Y., Zhang, X., Zheng, E., Yang, L., Yang,
649 Q., Qin, G., Zhou, J., and Shao, M.: Assessment of long tubing in measuring
650 atmospheric trace gases: applications on tall towers, *Environmental Science:
651 Atmospheres*, 3, 506-520,[10.1039/d2ea00110a](https://doi.org/10.1039/d2ea00110a) 2023.

652 Li, X., Wang, W., Yang, S., Cheng, Y., Zeng, L., Yu, X., Lu, S., Liu, Y., Hu, M., Xie,
653 S., Huang, X., Zhou, J., Shi, L., Xu, H., Lin, S., Liu, H., Feng, M., Song, D., Tan, Q.,
654 and Zhang, Y.: Ozone sensitivity regimes vary at different heights in the planetary
655 boundary layer, *Sci Total Environ*, 944,
656 173712,<https://doi.org/10.1016/j.scitotenv.2024.173712> 2024.

657 Liu, X., Deming, B., Pagonis, D., Day, D. A., Palm, B. B., Talukdar, R., Roberts, J. M.,
658 Veres, P. R., Krechmer, J. E., Thornton, J. A., de Gouw, J. A., Ziemann, P. J., and
659 Jimenez, J. L.: Effects of gas-wall interactions on measurements of semivolatile
660 compounds and small polar molecules, *Atmos. Meas. Tech.*, 12, 3137-
661 3149,[10.5194/amt-12-3137-2019](https://doi.org/10.5194/amt-12-3137-2019) 2019.

662 Liu, Y., Tang, G., Wang, Y., Cheng, M., Gao, J., and Wang, Y.: Spatiotemporal
663 differences in tropospheric ozone sensitivity and the impact of “dual carbon” goal,
664 *Science Bulletin*, 69, 422-425,<https://doi.org/10.1016/j.scib.2023.12.026> 2024a.

665 Liu, Y., Yin, S., Zhang, S., Ma, W., Zhang, X., Qiu, P., Li, C., Wang, G., Hou, D.,
666 Zhang, X., An, J., Sun, Y., Li, J., Zhang, Z., Chen, J., Tian, H., Liu, X., and Liu, L.:
667 Drivers and impacts of decreasing concentrations of atmospheric volatile organic
668 compounds (VOCs) in Beijing during 2016–2020, *Sci Total Environ*, 906,
669 167847,<https://doi.org/10.1016/j.scitotenv.2023.167847> 2024b.

670 Liu, Z., Pan, Y., Song, T., Hu, B., Wang, L., and Wang, Y.: Eddy covariance
671 measurements of ozone flux above and below a southern subtropical forest canopy, *Sci
672 Total Environ*, 791, 148338,<https://doi.org/10.1016/j.scitotenv.2021.148338> 2021.

673 Lu, K. D., Rohrer, F., Holland, F., Fuchs, H., Bohn, B., Brauers, T., Chang, C. C.,
674 Häseler, R., Hu, M., Kita, K., Kondo, Y., Li, X., Lou, S. R., Nehr, S., Shao, M., Zeng,

675 L. M., Wahner, A., Zhang, Y. H., and Hofzumahaus, A.: Observation and modelling of
676 OH and HO₂ concentrations in the Pearl River Delta 2006: a missing OH source in a
677 VOC rich atmosphere, *Atmos. Chem. Phys.*, 12, 1541-1569,10.5194/acp-12-1541-2012
678 2012.

679 Lu, Y., Pang, X., Lyu, Y., Li, J., Xing, B., Chen, J., Mao, Y., Shang, Q., and Wu, H.:
680 Characteristics and sources analysis of ambient volatile organic compounds in a typical
681 industrial park: Implications for ozone formation in 2022 Asian Games, *Sci Total*
682 *Environ*, 848, 157746,<https://doi.org/10.1016/j.scitotenv.2022.157746> 2022.

683 Ma, Z., Xu, H., Meng, W., Zhang, X., Xu, J., Liu, Q., and Wang, Y.: Vertical ozone
684 characteristics in urban boundary layer in Beijing, *Environ Monit Assess*, 185, 5449-
685 5460,10.1007/s10661-012-2958-5 2013.

686 Mo, Z., Shao, M., Wang, W., Liu, Y., Wang, M., and Lu, S.: Evaluation of biogenic
687 isoprene emissions and their contribution to ozone formation by ground-based
688 measurements in Beijing, China, *Sci Total Environ*, 627, 1485-
689 1494,<https://doi.org/10.1016/j.scitotenv.2018.01.336> 2018.

690 Mo, Z., Huang, S., Yuan, B., Pei, C., Song, Q., Qi, J., Wang, M., Wang, B., Wang, C.,
691 Li, M., Zhang, Q., and Shao, M.: Deriving emission fluxes of volatile organic
692 compounds from tower observation in the Pearl River Delta, China, *Sci Total Environ*,
693 741, 139763,<https://doi.org/10.1016/j.scitotenv.2020.139763> 2020.

694 Niu, H., Li, K., Chu, B., Su, W., and Li, J.: Heterogeneous Reactions between Toluene
695 and NO₂ on Mineral Particles under Simulated Atmospheric Conditions, *Environ Sci*
696 *Technol*, 51, 9596-9604,<https://doi.org/10.1021/acs.est.7b00194> 2017.

697 Ou, J., Zheng, J., Li, R., Huang, X., Zhong, Z., Zhong, L., and Lin, H.: Speciated OVOC
698 and VOC emission inventories and their implications for reactivity-based ozone control
699 strategy in the Pearl River Delta region, China, *Sci Total Environ*, 530-531, 393-
700 402,<https://doi.org/10.1016/j.scitotenv.2015.05.062> 2015.

701 Ou, J., Yuan, Z., Zheng, J., Huang, Z., Shao, M., Li, Z., Huang, X., Guo, H., and Louie,
702 P. K. K.: Ambient Ozone Control in a Photochemically Active Region: Short-Term
703 Despiking or Long-Term Attainment?, *Environ Sci Technol*, 50, 5720-
704 5728,<https://doi.org/10.1021/acs.est.6b00345> 2016.

705 Pagonis, D., Krechmer, J. E., de Gouw, J., Jimenez, J. L., and Ziemann, P. J.: Effects
706 of gas-wall partitioning in Teflon tubing and instrumentation on time-resolved
707 measurements of gas-phase organic compounds, *Atmos. Meas. Tech.*, 10, 4687-
708 4696,10.5194/amt-10-4687-2017 2017.

709 Perdignes, B. C., Lee, S., Cohen, R. C., Park, J.-H., and Min, K.-E.: Two Decades of
710 Changes in Summertime Ozone Production in California's South Coast Air Basin,
711 *Environ Sci Technol*, 56, 10586-10595,10.1021/acs.est.2c01026 2022.

712 Qi, J., Mo, Z., Yuan, B., Huang, S., Huangfu, Y., Wang, Z., Li, X., Yang, S., Wang,
713 W., Zhao, Y., Wang, X., Wang, W., Liu, K., and Shao, M.: An observation approach in
714 evaluation of ozone production to precursor changes during the COVID-19 lockdown,
715 *Atmos Environ*, 262, 118618,<https://doi.org/10.1016/j.atmosenv.2021.118618> 2021.

716 Sangiorgi, G., Ferrero, L., Perrone, M. G., Bolzacchini, E., Duane, M., and Larsen, B.
717 R.: Vertical distribution of hydrocarbons in the low troposphere below and above the

718 mixing height: Tethered balloon measurements in Milan, Italy, *Environ Pollut*, 159,
719 3545-3552, <https://doi.org/10.1016/j.envpol.2011.08.012> 2011.

720 Shao, M., Wang, W., Yuan, B., Parrish, D. D., Li, X., Lu, K., Wu, L., Wang, X., Mo,
721 Z., Yang, S., Peng, Y., Kuang, Y., Chen, W., Hu, M., Zeng, L., Su, H., Cheng, Y.,
722 Zheng, J., and Zhang, Y.: Quantifying the role of PM_{2.5} dropping in variations of
723 ground-level ozone: Inter-comparison between Beijing and Los Angeles, *Sci Total*
724 *Environ*, 147712, <https://doi.org/10.1016/j.scitotenv.2021.147712> 2021.

725 Song, X., Li, X.-B., Yuan, B., He, X., Chen, Y., Wang, S., Huangfu, Y., Peng, Y.,
726 Zhang, C., Liu, A., Yang, H., Liu, C., Li, J., and Shao, M.: Elucidating key factors in
727 regulating budgets of ozone and its precursors in atmospheric boundary layer, *npj*
728 *Climate and Atmospheric Science*, 7, 262, 10.1038/s41612-024-00818-8 2024.

729 Souri, A. H., Nowlan, C. R., Wolfe, G. M., Lamsal, L. N., Chan Miller, C. E., Abad, G.
730 G., Janz, S. J., Fried, A., Blake, D. R., Weinheimer, A. J., Diskin, G. S., Liu, X., and
731 Chance, K.: Revisiting the effectiveness of HCHO/NO₂ ratios for inferring ozone
732 sensitivity to its precursors using high resolution airborne remote sensing observations
733 in a high ozone episode during the KORUS-AQ campaign, *Atmos Environ*, 224,
734 117341, <https://doi.org/10.1016/j.atmosenv.2020.117341> 2020.

735 Sun, J., Wang, Y., Wu, F., Tang, G., Wang, L., Wang, Y., and Yang, Y.: Vertical
736 characteristics of VOCs in the lower troposphere over the North China Plain during
737 pollution periods, *Environ Pollut*, 236, 907-
738 915, <https://doi.org/10.1016/j.envpol.2017.10.051> 2018.

739 Tang, G., Zhu, X., Xin, J., Hu, B., Song, T., Sun, Y., Zhang, J., Wang, L., Cheng, M.,
740 Chao, N., Kong, L., Li, X., and Wang, Y.: Modelling study of boundary-layer ozone
741 over northern China - Part I: Ozone budget in summer, *Atmos Res*, 187, 128-
742 137, <https://doi.org/10.1016/j.atmosres.2016.10.017> 2017.

743 Velasco, E., Marquez, C., Bueno, E., Bernabe, R. M., Sanchez, A., Fentanes, O.,
744 Wohnrschimmel, H., Cardenas, B., Kamilla, A., Wakamatsu, S., and Molina, L. T.:
745 Vertical distribution of ozone and VOCs in the low boundary layer of Mexico City,
746 *Atmos. Chem. Phys.*, 8, 3061-3079, <https://doi.org/10.5194/acp-8-3061-2008> 2008.

747 Vo, T.-D.-H., Lin, C., Weng, C.-E., Yuan, C.-S., Lee, C.-W., Hung, C.-H., Bui, X.-T.,
748 Lo, K.-C., and Lin, J.-X.: Vertical stratification of volatile organic compounds and their
749 photochemical product formation potential in an industrial urban area, *J Environ*
750 *Manage*, 217, 327-336, <https://doi.org/10.1016/j.jenvman.2018.03.101> 2018.

751 Wang, C., Yuan, B., Wu, C., Wang, S., Qi, J., Wang, B., Wang, Z., Hu, W., Chen, W.,
752 Ye, C., Wang, W., Sun, Y., Wang, C., Huang, S., Song, W., Wang, X., Yang, S., Zhang,
753 S., Xu, W., Ma, N., Zhang, Z., Jiang, B., Su, H., Cheng, Y., Wang, X., and Shao, M.:
754 Measurements of higher alkanes using NO⁺ chemical ionization in PTR-ToF-MS:
755 important contributions of higher alkanes to secondary organic aerosols in China,
756 *Atmos. Chem. Phys.*, 20, 14123-14138, <https://doi.org/10.5194/acp-20-14123-2020>
757 2020a.

758 Wang, H., Ma, X., Tan, Z., Wang, H., Chen, X., Chen, S., Gao, Y., Liu, Y., Liu, Y.,
759 Yang, X., Yuan, B., Zeng, L., Huang, C., Lu, K., and Zhang, Y.: Anthropogenic
760 monoterpenes aggravating ozone pollution, *Natl Sci Rev*, 9,
761 nwac103, 10.1093/nsr/nwac103 2022a.

762 Wang, N., Lyu, X., Deng, X., Huang, X., Jiang, F., and Ding, A.: Aggravating O₃
763 pollution due to NO_x emission control in eastern China, *Sci Total Environ*, 677, 732-
764 744,<https://doi.org/10.1016/j.scitotenv.2019.04.388> 2019.

765 Wang, N., Huang, X., Xu, J., Wang, T., Tan, Z.-m., and Ding, A.: Typhoon-boosted
766 biogenic emission aggravates cross-regional ozone pollution in China, *Science*
767 *Advances*, 8, eabl6166,doi:10.1126/sciadv.abl6166 2022b.

768 Wang, W., Qi, J., Zhou, J., Yuan, B., Peng, Y., Wang, S., Yang, S., Williams, J., Sinha,
769 V., and Shao, M.: The improved comparative reactivity method (ICRM): measurements
770 of OH reactivity under high-NO_x conditions in ambient air, *Atmos. Meas. Tech.*, 14,
771 2285-2298,10.5194/amt-14-2285-2021 2021a.

772 Wang, W., Yuan, B., Peng, Y., Su, H., Cheng, Y., Yang, S., Wu, C., Qi, J., Bao, F.,
773 Huangfu, Y., Wang, C., Ye, C., Wang, Z., Wang, B., Wang, X., Song, W., Hu, W.,
774 Cheng, P., Zhu, M., Zheng, J., and Shao, M.: Direct observations indicate
775 photodegradable oxygenated volatile organic compounds (OVOCs) as larger
776 contributors to radicals and ozone production in the atmosphere, *Atmos. Chem. Phys.*,
777 22, 4117-4128,10.5194/acp-22-4117-2022 2022c.

778 Wang, W., Li, X., Cheng, Y., Parrish, D. D., Ni, R., Tan, Z., Liu, Y., Lu, S., Wu, Y.,
779 Chen, S., Lu, K., Hu, M., Zeng, L., Shao, M., Huang, C., Tian, X., Leung, K. M., Chen,
780 L., Fan, M., Zhang, Q., Rohrer, F., Wahner, A., Pöschl, U., Su, H., and Zhang, Y.:
781 Ozone pollution mitigation strategy informed by long-term trends of atmospheric
782 oxidation capacity, *Nature Geoscience*, 17, 20-25,10.1038/s41561-023-01334-9 2024.

783 Wang, Y., Wang, Y., Tang, G., Yang, Y., Li, X., Yao, D., Wu, S., Kang, Y., Wang, M.,
784 and Wang, Y.: High gaseous carbonyl concentrations in the upper boundary layer in
785 Shijiazhuang, China, *Sci Total Environ*, 799,
786 149438,<https://doi.org/10.1016/j.scitotenv.2021.149438> 2021b.

787 Wang, Y. H., Gao, W. K., Wang, S., Song, T., Gong, Z. Y., Ji, D. S., Wang, L. L., Liu,
788 Z. R., Tang, G. Q., Huo, Y. F., Tian, S. L., Li, J. Y., Li, M. G., Yang, Y., Chu, B. W.,
789 Petaja, T., Kerminen, V. M., He, H., Hao, J. M., Kulmala, M., Wang, Y. S., and Zhang,
790 Y. H.: Contrasting trends of PM_{2.5} and surface-ozone concentrations in China from
791 2013 to 2017, *National Science Review*, 7, 1331-
792 1339,<https://doi.org/10.1093/nsr/nwaa032> 2020b.

793 Wolfe, G. M., Marvin, M. R., Roberts, S. J., Travis, K. R., and Liao, J.: The Framework
794 for 0-D Atmospheric Modeling (F0AM) v3.1, *Geoscientific Model Development*, 9,
795 3309-3319,10.5194/gmd-9-3309-2016 2016.

796 Wu, C., Wang, C., Wang, S., Wang, W., Yuan, B., Qi, J., Wang, B., Wang, H., Wang,
797 C., Song, W., Wang, X., Hu, W., Lou, S., Ye, C., Peng, Y., Wang, Z., Huangfu, Y., Xie,
798 Y., Zhu, M., Zheng, J., Wang, X., Jiang, B., Zhang, Z., and Shao, M.: Measurement
799 report: Important contributions of oxygenated compounds to emissions and chemistry
800 of volatile organic compounds in urban air, *Atmos. Chem. Phys.*, 20, 14769-
801 14785,<https://doi.org/10.5194/acp-20-14769-2020> 2020.

802 Yang, Q., Li, X. B., Yuan, B., Zhang, X., Huangfu, Y., Yang, L., He, X., Qi, J., and
803 Shao, M.: Measurement report: Enhanced photochemical formation of formic and
804 isocyanic acids in urban regions aloft – insights from tower-based online gradient
805 measurements, *Atmos. Chem. Phys.*, 24, 6865-6882,10.5194/acp-24-6865-2024 2024a.

806 Yang, S., Yuan, B., Peng, Y., Huang, S., Chen, W., Hu, W., Pei, C., Zhou, J., Parrish,
807 D. D., Wang, W., He, X., Cheng, C., Li, X. B., Yang, X., Song, Y., Wang, H., Qi, J.,
808 Wang, B., Wang, C., Wang, C., Wang, Z., Li, T., Zheng, E., Wang, S., Wu, C., Cai, M.,
809 Ye, C., Song, W., Cheng, P., Chen, D., Wang, X., Zhang, Z., Wang, X., Zheng, J., and
810 Shao, M.: The formation and mitigation of nitrate pollution: comparison between urban
811 and suburban environments, *Atmos. Chem. Phys.*, 22, 4539-4556, [10.5194/acp-22-](https://doi.org/10.5194/acp-22-4539-2022)
812 [4539-2022](https://doi.org/10.5194/acp-22-4539-2022) 2022.

813 Yang, X., Wang, H., Lu, K., Ma, X., Tan, Z., Long, B., Chen, X., Li, C., Zhai, T., Li,
814 Y., Qu, K., Xia, Y., Zhang, Y., Li, X., Chen, S., Dong, H., Zeng, L., and Zhang, Y.:
815 Reactive aldehyde chemistry explains the missing source of hydroxyl radicals, *Nature*
816 *Communications*, 15, 1648, [10.1038/s41467-024-45885-w](https://doi.org/10.1038/s41467-024-45885-w) 2024b.

817 Ye, C., Yuan, B., Lin, Y., Wang, Z., Hu, W., Li, T., Chen, W., Wu, C., Wang, C., Huang,
818 S., Qi, J., Wang, B., Wang, C., Song, W., Wang, X., Zheng, E., Krechmer, J. E., Ye, P.,
819 Zhang, Z., Wang, X., Worsnop, D. R., and Shao, M.: Chemical characterization of
820 oxygenated organic compounds in the gas phase and particle phase using iodide CIMS
821 with FIGAERO in urban air, *Atmos. Chem. Phys.*, 21, 8455-
822 [8478,https://doi.org/10.5194/acp-21-8455-2021](https://doi.org/10.5194/acp-21-8455-2021) 2021.

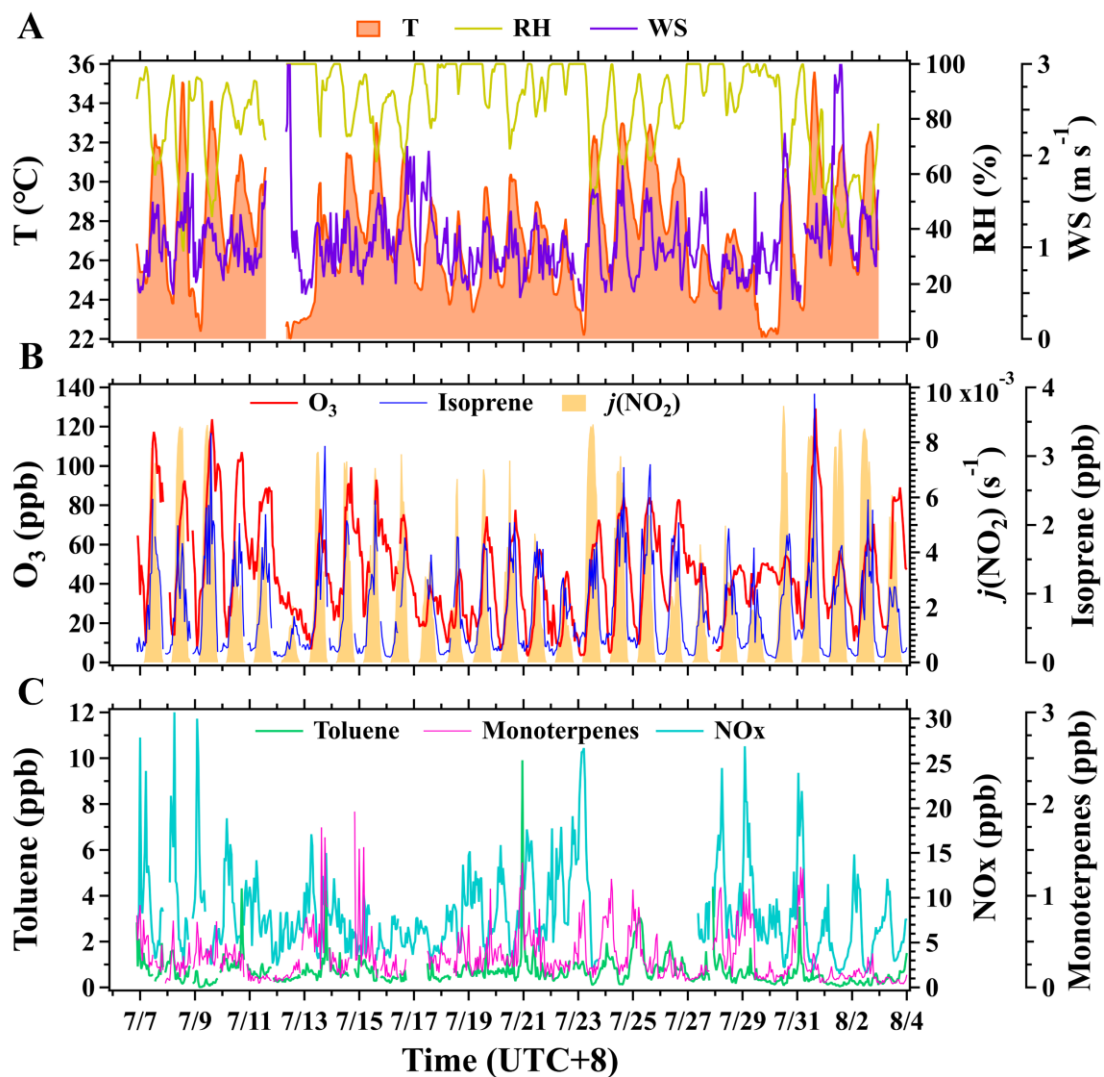
823 Yeo, M. J., and Kim, Y. P.: Long-term trends of surface ozone in Korea, *Journal of*
824 *Cleaner Production*, 294, 125352, <https://doi.org/10.1016/j.jclepro.2020.125352> 2021.

825 Yuan, B., Koss, A. R., Warneke, C., Coggon, M., Sekimoto, K., and de Gouw, J. A.:
826 Proton-Transfer-Reaction Mass Spectrometry: Applications in Atmospheric Sciences,
827 *Chem Rev*, 117, 13187-13229, <https://doi.org/10.1021/acs.chemrev.7b00325> 2017.

828 Zhang, K., Xiu, G., Zhou, L., Bian, Q., Duan, Y., Fei, D., Wang, D., and Fu, Q.: Vertical
829 distribution of volatile organic compounds within the lower troposphere in late spring
830 of Shanghai, *Atmos Environ*, 186, 150-
831 [157,https://doi.org/10.1016/j.atmosenv.2018.03.044](https://doi.org/10.1016/j.atmosenv.2018.03.044) 2018.

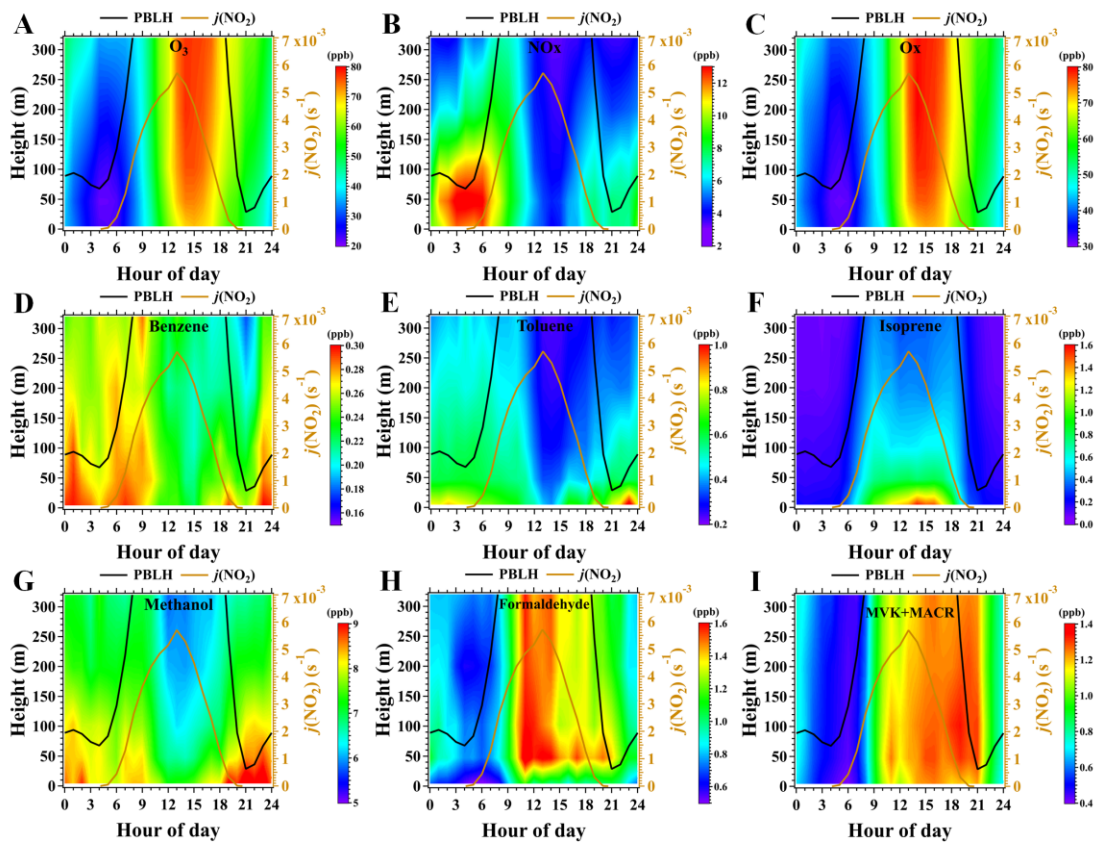
832 Zhang, Y., Xue, L., Mu, J., Chen, T., Li, H., Gao, J., and Wang, W.: Developing the
833 Maximum Incremental Reactivity for Volatile Organic Compounds in Major Cities of
834 Central-Eastern China, *Journal of Geophysical Research: Atmospheres*, 127,
835 [e2022JD037296,https://doi.org/10.1029/2022JD037296](https://doi.org/10.1029/2022JD037296) 2022.

836 Zhao, M., Zhang, Y., Pei, C., Chen, T., Mu, J., Liu, Y., Wang, Y., Wang, W., and Xue,
837 L.: Worsening ozone air pollution with reduced NO_x and VOCs in the Pearl River Delta
838 region in autumn 2019: Implications for national control policy in China, *J Environ*
839 *Manage*, 324, 116327, <https://doi.org/10.1016/j.jenvman.2022.116327> 2022.



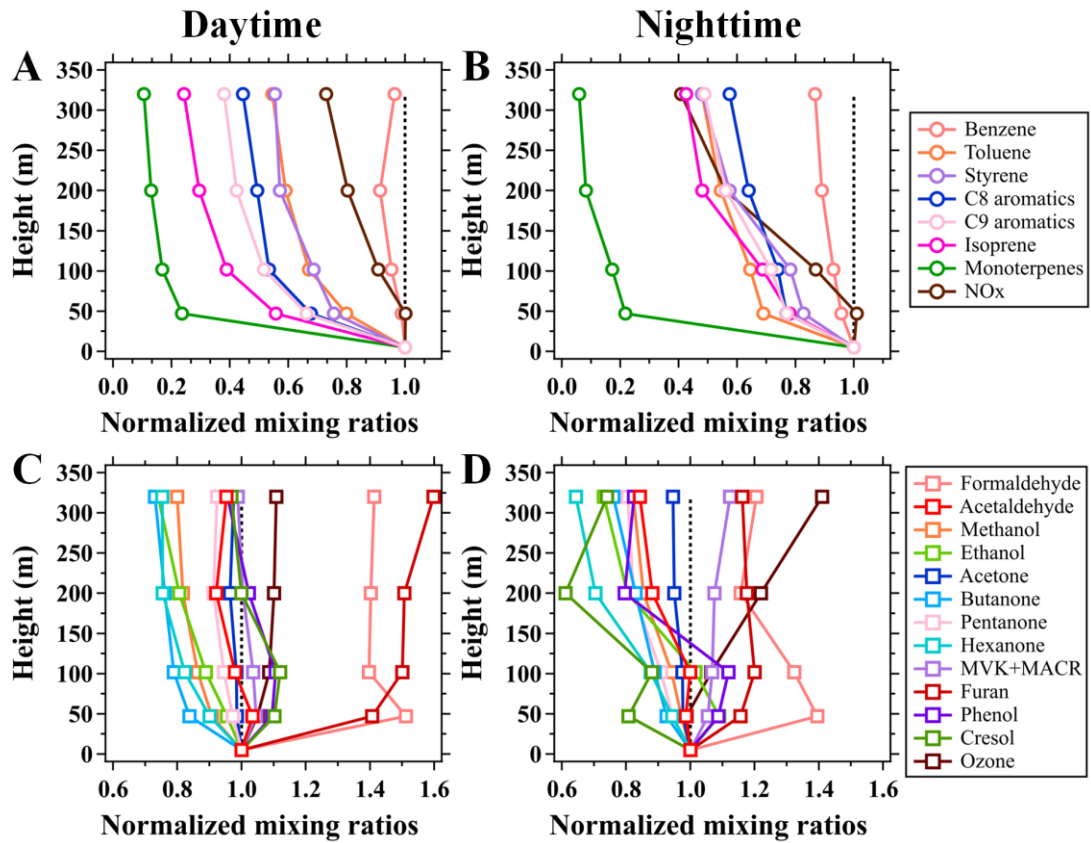
840

841 **Figure 1.** Time series of hourly mean air temperature (T), relative humidity (RH), wind
 842 speed (WS), and mixing ratios of surface ozone, NO_x, and VOC species along with
 843 $j(\text{NO}_2)$ at the BMT site during the campaign. Meteorological parameters were measured
 844 at 8 m above ground level and mixing ratios of ozone and its selected precursors were
 845 measured at 5 m above ground level.



846

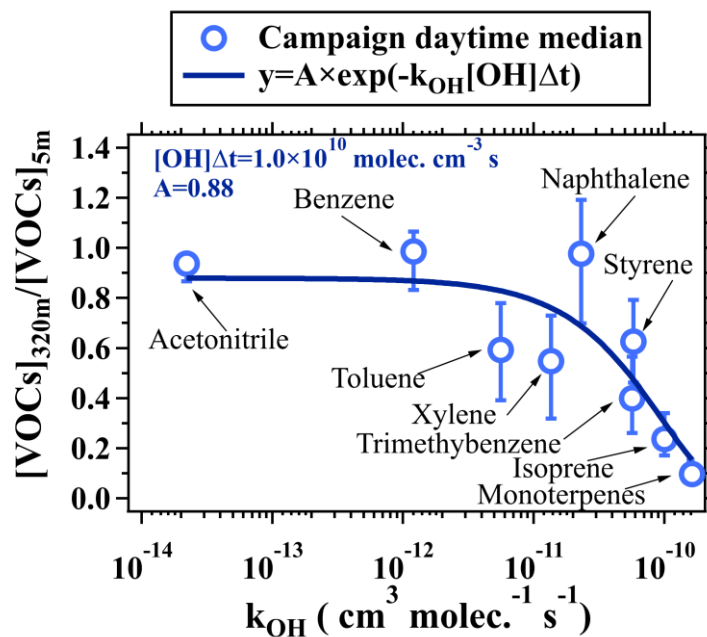
847 **Figure 2.** Average diurnal and vertical variations in mixing ratios ozone, NO_x, Ox
 848 (O₃+NO₂), and six selected VOC species along with the average diurnal profiles of
 849 PBLH and $j(\text{NO}_2)$ during the campaign. The figures were obtained by linearly
 850 interpolating the data at the five inlet heights on both altitude and temporal scales.



851

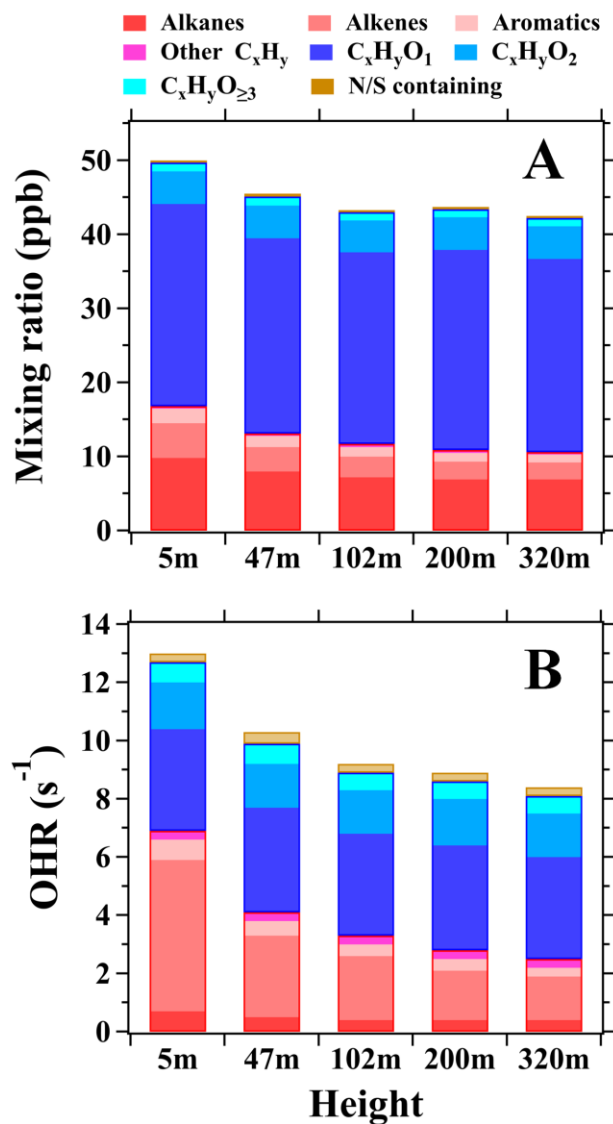
852 **Figure 3.** Average vertical profiles of (A-B) NMHCs and NO_x, (C-D) OVOCs and O₃
 853 during the daytime (11:00-16:00 LT) and nighttime (23:00-04:00 LT) of the campaign.

854 The mixing ratios of the chemical species measured above 5 m are normalized to those
 855 at 5 m.



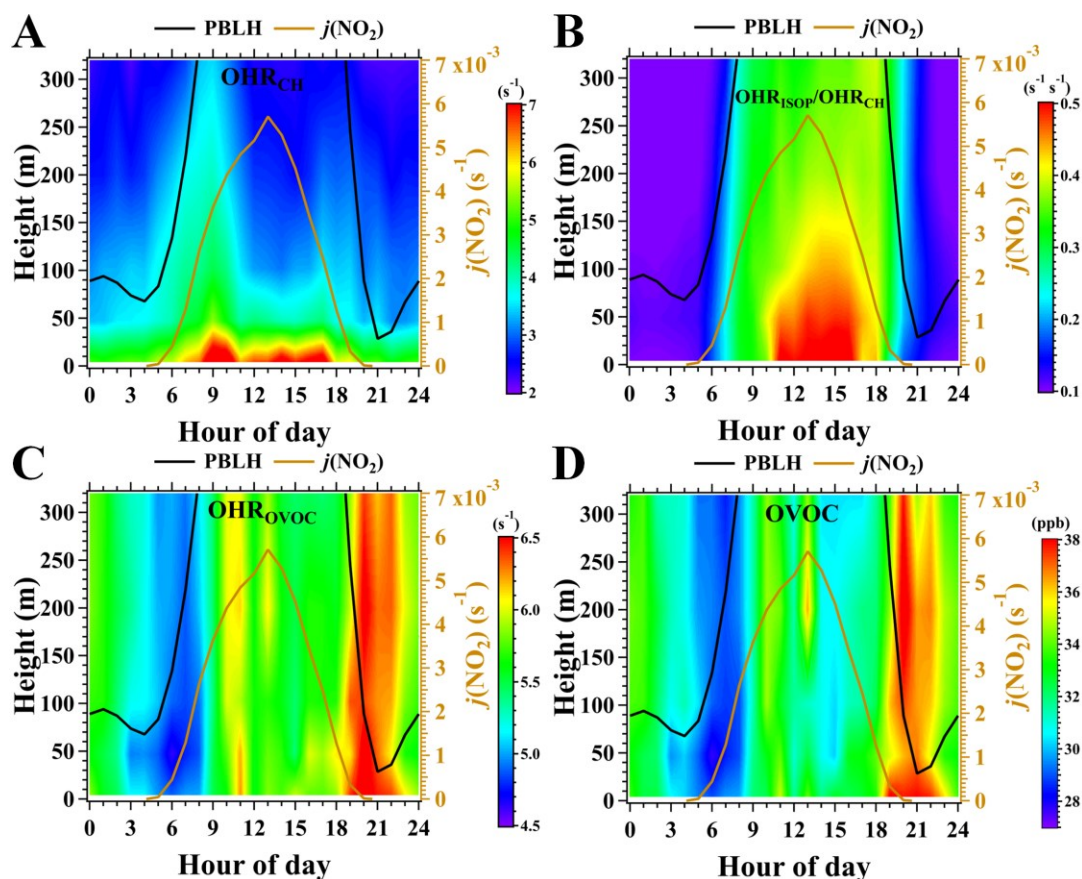
856

857 **Figure 4.** The change in ratios of NMHC concentrations (including acetonitrile)
 858 between 320 m and 5 m as a function of k_{OH} . The vertically-resolved measurements of
 859 VOCs made on the BMT in daytime during the campaign were used for analysis.
 860 Hollow markers represent median values and error bars indicate the range between 25th
 861 and 75th percentiles.



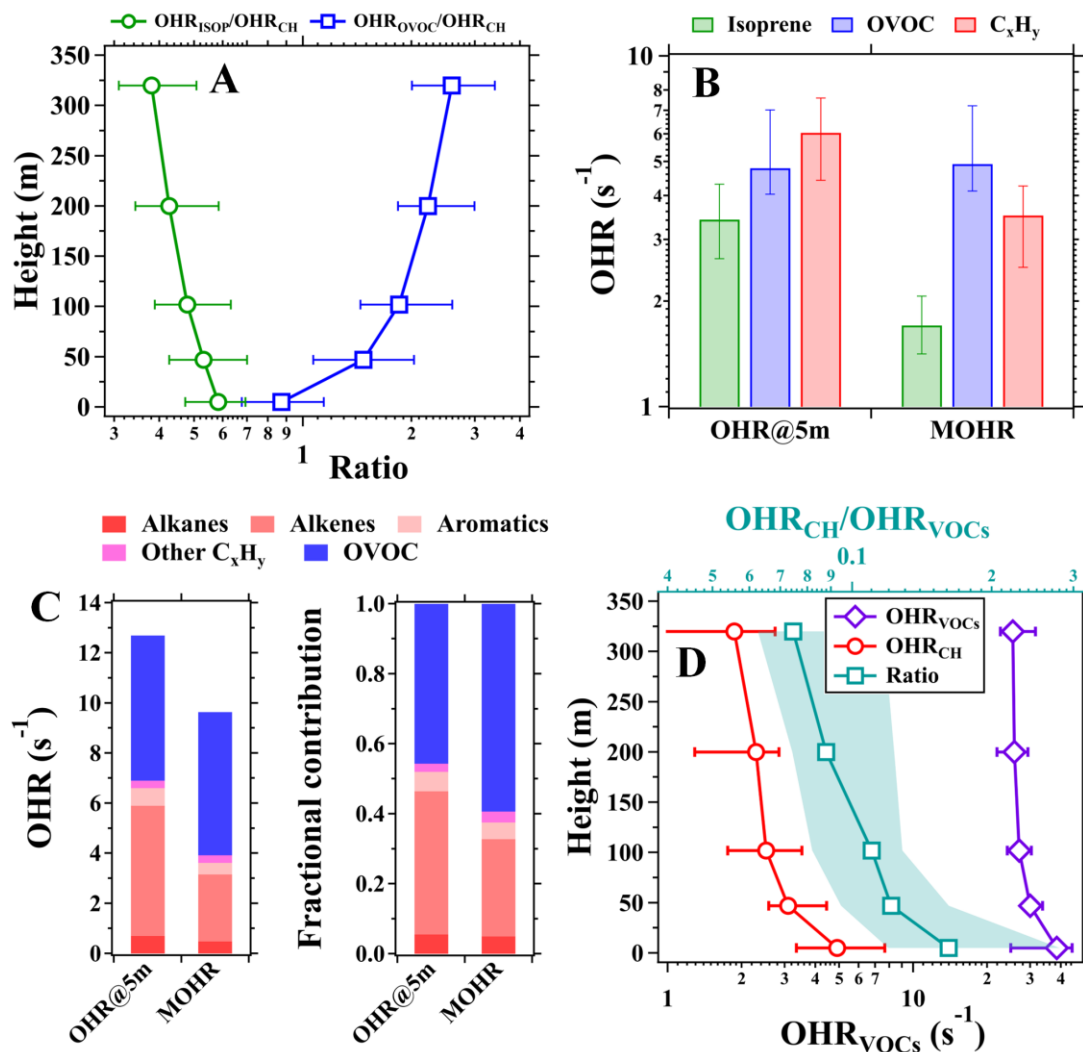
862

863 **Figure 5.** (A) Mean mixing ratios and (B) OHRs of different VOC categories at the five
 864 inlet heights in daytime during the campaign.



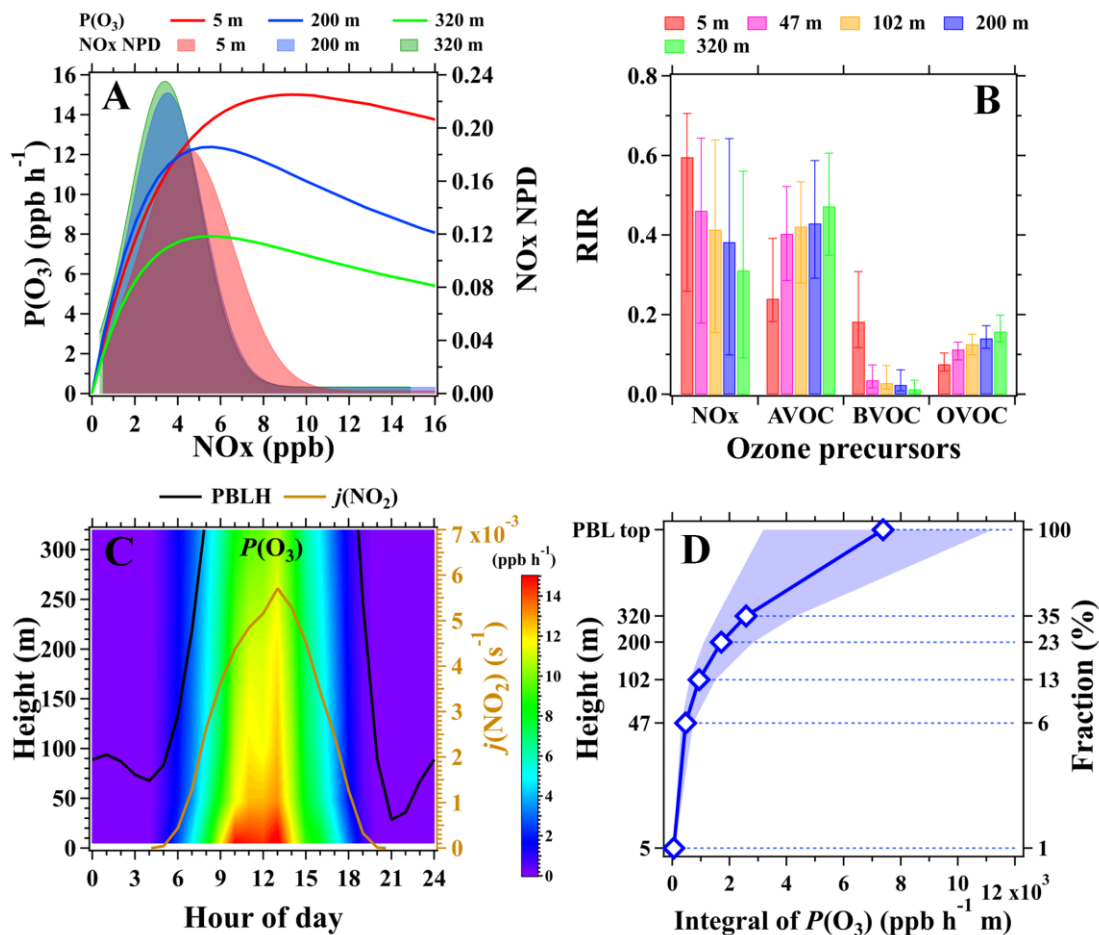
865

866 **Figure 6.** (A-B) Average diurnal and vertical variations in OHRs of C_xH_y and the OHR
 867 ratios of isoprene to C_xH_y ($\text{OHR}_{\text{ISOP}}/\text{OHR}_{\text{CH}}$) during the campaign. (C-D) Average
 868 diurnal and vertical variations in mixing ratios and OHRs of OVOC. ISOP refers to
 869 isoprene. The figures were obtained by linearly interpolating the data at the five
 870 measurement heights on both altitude and temporal scales.



871

872 **Figure 7.** (A) Average vertical profiles of OHR ratios of isoprene to C_xH_y
 873 (OHR_{ISOP}/OHR_{CH}) and OVOC to NMHC (OHR_{OVOC}/OHR_{CH}). (B) Median values of
 874 the OHR at 5 m and the mean OHR (MOHR) between 5 m and 320 m for isoprene,
 875 OVOC, and C_xH_y . (C) Mean contributions of different VOC categories to the MOHR
 876 below 320 m and the OHR at 5 m. (D) Vertical profiles of the measured OHR_{VOCs} and
 877 the calculated OHR_{CH} (bottom axis) and the OHR_{CH}/OHR_{VOCs} ratios (top axis) during
 878 July 28-31, 2021. The data used for analysis in panels A-D was within the time window
 879 from 11:00 to 16:00 LT during the campaign. Markers in panels A and D represent
 880 median values. Shaded areas and error bars in panels A, B, and D indicate the range
 881 between 25th and 75th percentiles.



882

883 **Figure 8.** (A) Left axis: average dependence of $P(\text{O}_3)$ on NO_x concentrations in
 884 daytime during the campaign; Right axis: normalized probability density (NPD) of
 885 NO_x mixing ratios in daytime at the three inlet heights. (B) Median RIR values of
 886 photochemical ozone formation to changes in NO_x , AVOC (NMHCs excluding BVOC),
 887 BVOC (isoprene), and OVOC (nine OVOC species in Table S1) at the five inlet heights;
 888 Error bars indicate the range between 25th and 75th percentiles. (C) Average diurnal and
 889 vertical variations in $P(\text{O}_3)$ during the campaign; The figure was obtained by linearly
 890 interpolating the data at the five measurement heights on both altitude and temporal
 891 scales. (D) The vertical profile of the integral of $P(\text{O}_3)$ in daytime during the campaign;
 892 Markers indicate median values and Shaded areas indicate the range between 25th and
 893 75th percentiles.